




Article

One-Step Preparation of High Performance TiO₂/CNT/CQD Nanocomposites Bactericidal Coating with Ultrasonic Radiation

Jin Xiang^{1,2}, Shuchang Wang³, Yuanxin Cao³, Lining Fang⁴, Wei Ke³, Hui Guo^{3,*}, Baoyu Duan^{5,*},
Wenhe Yu⁶, Liang Li⁷ and Zilong Zhao^{3,*}

¹ Department of Mechanics, Jinzhong University, Jinzhong 030619, China

² Leo Group Pump (Zhejiang) Co., Ltd., Taizhou 318000, China

³ School of Chemical Engineering and Technology, Sun Yat-sen University, Zhuhai 519082, China

⁴ Department of Environmental Science, Hebei University of Environmental Engineering, Qinghuangdao 066000, China

⁵ College of Locomotive and Rolling Stock Engineering, Dalian Jiaotong University, Dalian 116028, China

⁶ Beijing Key Laboratory of Materials Utilization of Nonmetallic Minerals and Solid Wastes, National Laboratory of Mineral Materials, School of Materials Science and Technology, China University of Geosciences, Beijing 100083, China

⁷ School of Physics, Engineering and Computer Science, University of Hertfordshire, Hatfield AL10 9AB, UK

* Correspondence: guoh37@mail.sysu.edu.cn (H.G.); duanby83@163.com (B.D.);

zhaozlong@mail.sysu.edu.cn (Z.Z.)

Abstract: As an environmental semiconductor material, TiO₂ has important applications in the fields of environmental protection and water treatment. The preparation of P25 particles into nano-functional material films with a high specific surface area has always been a bottleneck limiting its large-scale application. In this paper, a one-step method of preparing TiO₂ nanocomposites by doping carbon nanotube (CNT) and carbon quantum dots (CQD) with tetrabutyltitanate and P25 TiO₂ under ultrasonic radiation is proposed to synthesize a novel antifouling material, which both eliminates the bacterium of Escherichia coli and shows good photoelectric properties, indicating a great value for the industrial promotion of TiO₂/CNT. This mesoporous composite exhibits a high specific surface area of 78.07 M²/g (BET) and a tested pore width range within 10–120 nm. The surface morphology of this composite is characterized by TEM and the microstructure is characterized through XRD. This preparation method can fabricate P25 particles into a nano-functional material film with a high specific surface area at a very low cost.

Keywords: TiO₂; carbon quantum dots; one-step synthesis; ultrasonic radiation; carbon nanotube; mesoporous nanocomposites



Citation: Xiang, J.; Wang, S.; Cao, Y.; Fang, L.; Ke, W.; Guo, H.; Duan, B.; Yu, W.; Li, L.; Zhao, Z. One-Step Preparation of High Performance TiO₂/CNT/CQD Nanocomposites Bactericidal Coating with Ultrasonic Radiation. *Coatings* **2023**, *13*, 145. <https://doi.org/10.3390/coatings13010145>

Academic Editor: Joaquim Carneiro

Received: 27 November 2022

Revised: 2 January 2023

Accepted: 3 January 2023

Published: 11 January 2023



Copyright: © 2023 by the authors. Licensee MDPI, Basel, Switzerland. This article is an open access article distributed under the terms and conditions of the Creative Commons Attribution (CC BY) license (<https://creativecommons.org/licenses/by/4.0/>).

1. Introduction

Photosynthesis in nature achieves a highly efficient solar energy conversion mainly through combining several different molecules to arrange the nanoscale, which indicates the importance of a technique for the site-selective coupling of different materials to realize artificially efficient devices [1–3]. TiO₂ is a kind of safe, stable, and cheap material, which has attracted significant research interest [4–9]. Photo-catalytic reactions on the semi-conductive surfaces of TiO₂ materials are widely investigated and reported for the purposes of (1) water splitting to produce H₂ and (2) eliminating pollutants from water and air [10–15]. Obviously, the direct splitting of water molecules through Photo-electrochemical (PEC) processes is a sustainable green approach to convert water and sunlight to hydrogen and oxygen to achieve [16,17]. Much effort has been made in the selection of efficient stable semiconductor materials to build PEC cells, thus bringing silicon (Si), III–V compounds, and various oxides into sight [18–23]. In the first-row of transition metal oxides, TiO₂ is a poor water oxidation catalyst with a large over potential for the sluggish kinetics and oxygen

evolution reaction [14]. Hence, it is essential to develop a TiO₂-based visible light responsive photo-catalyst, and much work has been done to develop “second-generation” TiO₂ and other narrow band gap semiconductors to absorb visible light [17,24–27]. Though nano-sized particles could be prepared by the sol-gel method for the film’s preparation, the size of the particles is difficult to control [28–32]. The introduction of the graphene/graphene derivatives (including graphene oxide (GO) and other forms of functionalized graphene), the 3D single atom thick carbon layer, as the framework of the membrane, enables the morphology of the nanostructured materials to be extended from 1D to 0D (nanoparticles). The range of the nanostructured materials chosen is extended from only the photocatalytic materials (TiO₂, ZnO, CoS, CdS, CdSe, MoO_x, etc.) to other functional materials (MnO₂ for oxidation, Ag for disinfection, Pt for catalysis, etc.). Applying the 3D graphene-based nanocomposite multicomposite membrane with an expected thickness < 100 nm for the desalination applications will potentially create a new and promising industrial sector, and these applications are still undeveloped.

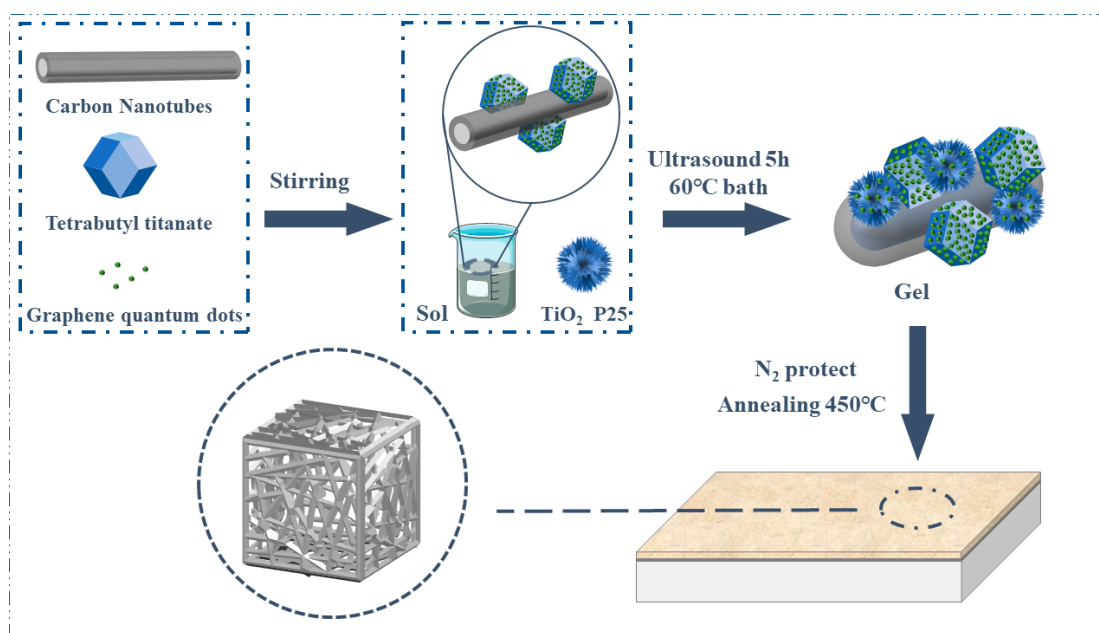
It is known that TiO₂ is a wide bandgap semiconductor, with a low-to-moderate response rate to sunlight, and research has focused on reducing the absorption edge energy to improve the utilization of sunlight [33,34]. Moreover, the large specific area of mesoporous TiO₂ nanoparticles is another favorable factor for generating large quantities of active sites for a photocatalytic reaction, which has taken place on the surface of the photocatalyst [35]. Additionally, the preparation of P25 particles into nano-functional material films with a high specific surface area has always been a bottleneck limiting its large-scale application.

In this work, sol was prepared with tetrabutyl titanate; commercial P25 TiO₂ was added to ensure the uniformity of the nanoparticles; and CNT and CQD were doped to improve the light absorptivity of the semi-conductive materials. CQD also contributed to the gel’s formation.

2. Experimental Section

2.1. Synthesis

Ti(O-*i*-C₄H₉)₄ (TB, Aladdin, AR) (≥98% Ti) and ethanol absolute (EtOH, Aladdin, Nanjing, China, AR) were blended with a 5% (wt.) multi-wall carbon nanotube (Nano-Com Shanghai, China,) average particle size 10–20 nm) to make a mixture. Hydrochloride acid was added as a catalyst to enhance the hydrolysis rate. Commercial P25 TiO₂ (Innochem) particles with an average particle size of 25 nm were dispersed into the Ti-based sol at 0.2 g/mL in vigorous magnetic stirring for 30 min. GQD nanomaterials with a diameter of 15 nm were purchased from Aladdin (G196610-100 mL). GQDs were dispersed into the tetra-*n*-butyl orthotitanate at 80 mg/mL in vigorous magnetic stirring for more than 5 min. The mixture was then stirred via vigorous mechanical stirring and subsequently placed in an 80 °C water bath with an ultrasonic (Dakou, Kongshan, China, KQ-300VDE, 45 kHz) for 5 h. After that, the sonicated mixture was dried overnight at a temperature of 80 °C and then calcined in an Ar atmosphere at 450 °C for 6 h before the grounding procedure to obtain an anatase phase. The schematic of the formation of the mesoporous TiO₂/CNT/CQD nanocomposites membrane is shown in Scheme 1.



Scheme 1. Formation of mesoporous TiO₂/CNT/CQD nanocomposites membrane by sol-gel ultrasonic irradiation method.

2.2. Characterization

Various characterizing techniques, including a transmission electron microscope (FEI Talos-F200S TEM), pore structure determination (Brunauer–Emmett–Teller, BET method), and X-ray diffraction (XRD), were applied to analyze the material. A transmission electron microscope (JEOL, JEOL-2100F, Tokyo, Japan) was used to characterize the microstructure. UV–vis DRS was performed on a spectrophotometer (Lambda750, PerkinElmer, Inc., Waltham, MA, USA). The absorbance was tested using a UV–vis spectro-photometer (722, Weimipai Technology Co., Ltd., Hangzhou, China). The light absorption properties were measured using a Fourier Infrared Instrument (PerkinElmer Spectrum, Akron, OH, USA). The absorbance properties were measured using the Zolix SS150 (Zolix Instruments Co., Ltd., Beijing, China). The light intensity and photoluminescence spectrum's structure were determined using a fluorescence spectrometer (F-4500, Hitachi, Ibaraki, Japan). The photo-electrochemical properties were measured on an electrochemical workstation (Chenhua, CHI660E, Shanghai, China).

2.3. Antibacterial Tests

To test the materials with the bacterium of *Escherichia coli*, typically, the sample (10 mg) was added to 10 mL of pure water to make a TiO₂ solution (solution T) with TiO₂ suspended within. To remove the microorganisms from the system, the whole set was sterilized in an automatic high-temperature sterilization pot. Then, using a conventional bacterial solution with its original concentrate of 1.15 g/L, a 0.01% diluted solution was prepared and 100 µL of this solution was added into the TiO₂ solution (solution T) as a source of *Escherichia coli*. The mixture was irradiated under 34.4 Klux solar light for 1 h. After lighting, the antibacterial solution was coated on the prepared solid medium (10 g of pancreatic protein, 5 g of yeast powder, 10 g of NaCl, and 20 g of agar diluted with 1 L of pure water) and was tested after 8 h for its anti-bacterial performance.

3. Results and Discussion

Figure 1 presents the results of the BET test of the TiO₂/CNT/CQD nanocomposites. The surface area of TiO₂/CNT/CQD is as high as 78.07 m²/g and the pore width range is 10–120 nm, indicating that an ultrasonic radiation treatment is a useful technique to prepare mesoporous materials [36–39]. Bai has reported that the surface area of the TiO₂/CNT

mesoporous composite material is $42.90 \text{ m}^2/\text{g}$ [40]. Therefore, the doping of CQD is beneficial to increase the surface of the $\text{TiO}_2/\text{CNT}/\text{CQD}$ nanocomposites. It attributes to the small particle size.

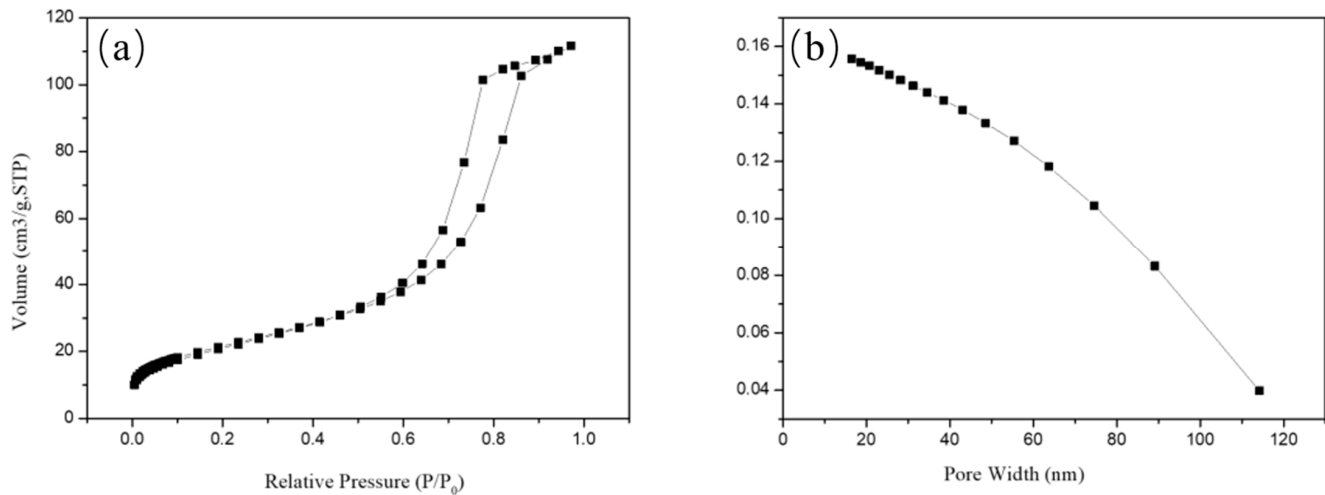


Figure 1. Isotherms of nitrogen adsorption–desorption and pore width of the $\text{TiO}_2/\text{CNT}/\text{CQD}$ mesoporous composite. (a) Nitrogen adsorption–desorption isotherms and pore width of $\text{TiO}_2/\text{CNT}/\text{CQD}$, (b) aperture distribution map.

Figure 2 shows the energy disperse spectroscopy (EDS) mapping results of the $\text{TiO}_2/\text{CNT}/\text{CQD}$ mesoporous nanocomposites prepared under ultrasonic radiation. Small TiO_2 particles appear to cluster around the carbon nanotube, indicating that the nanotube is a sufficient support material for a better TiO_2/CNT dispersion in this specific preparation. Although the composite interface between TiO_2 and the carbon nanotube, which appears to be a loose one, needs to be further improved, the doping of TiO_2 with CNT and CQD obviously improves the dispersion of TiO_2 as well as promotes the formation of hetero junctions at the TiO_2 –CNT interface, which favors the improvement of the absorption efficiency of visible light [41,42].

The TEM results of $\text{TiO}_2/\text{CNT}/\text{CQD}$ prepared with the ultrasonic treatment are shown in Figure 3. Figure 3a depicts the agglomeration of small particles in the $\text{TiO}_2/\text{CNT}/\text{CQD}$ mesoporous nanocomposites. In Figure 3b, the interface between the two main phases, namely the TiO_2 and the CNT, has been remarkably enhanced through a high temperature. The high-resolution diagrams, Figure 3c,d, correspond to anatase TiO_2 [43,44], which clearly represent the relevant information at the atomic scale. Figure 3e,f are high-resolution TEM diagrams of CQD. From Figure 4, it can be seen that the morphology and spacing between the crystal planes are CQD, and CQD is successfully doped into P25 and CNT by sol-gel, but there is only a small amount of reunion.

The FTIR spectra have indicated that the characteristic bands at 3400 cm^{-1} and 1630 cm^{-1} correspond to the surface water and hydroxyl group [45]. Figure 4 shows the XRD results of the $\text{TiO}_2/\text{CNT}/\text{CQD}$ mesoporous composite. As shown in Figure 4, it can be found that the $\text{TiO}_2/\text{CNT}/\text{CQD}$ mesoporous composite is an obvious anatase phase and C phase, which is conducive to improving the photoelectric properties of the material. TiO_2 nanoparticles have attracted great interest because of their special physical and chemical properties, especially as photocatalytic oxidation catalysts in corresponding device materials and environmental pollution control [46].

Marine fouling is a critical issue in modern marine science and technology, which strictly determines marine transportation and farming. The existing antifouling approaches, such as antifouling hydrogel coatings and organic tin coating [47–49], always demonstrate an unsatisfactory performance. In our system, the material shows the CV curves and anti-bacterial properties of the control, TiO_2/CNT and $\text{TiO}_2/\text{CNT}/\text{CQD}$, using *Escherichia*

coli bacteria (Figure 5). Comparing the bacteriostasis processes uses TiO_2/CNT (Figure 5c) and $\text{TiO}_2/\text{CNT}/\text{CQD}$ (Figure 5d) as anti-bacterium agents, respectively. In this experiment, obviously, the number of *Escherichia coli* bacterial colonies in Petri dishes all increased with time. The sample (c) with $\text{TiO}_2/\text{CNT}/\text{CQD}$ as an anti-bacterium agent got the bacterium of *Escherichia coli* under control, while the sample using TiO_2 as an anti-bacterium agent just grew more bacterial colonies, indicating that doping TiO_2 with CNT and CQD contributes to boosting the TiO_2 s performance in an environmental pollution control.

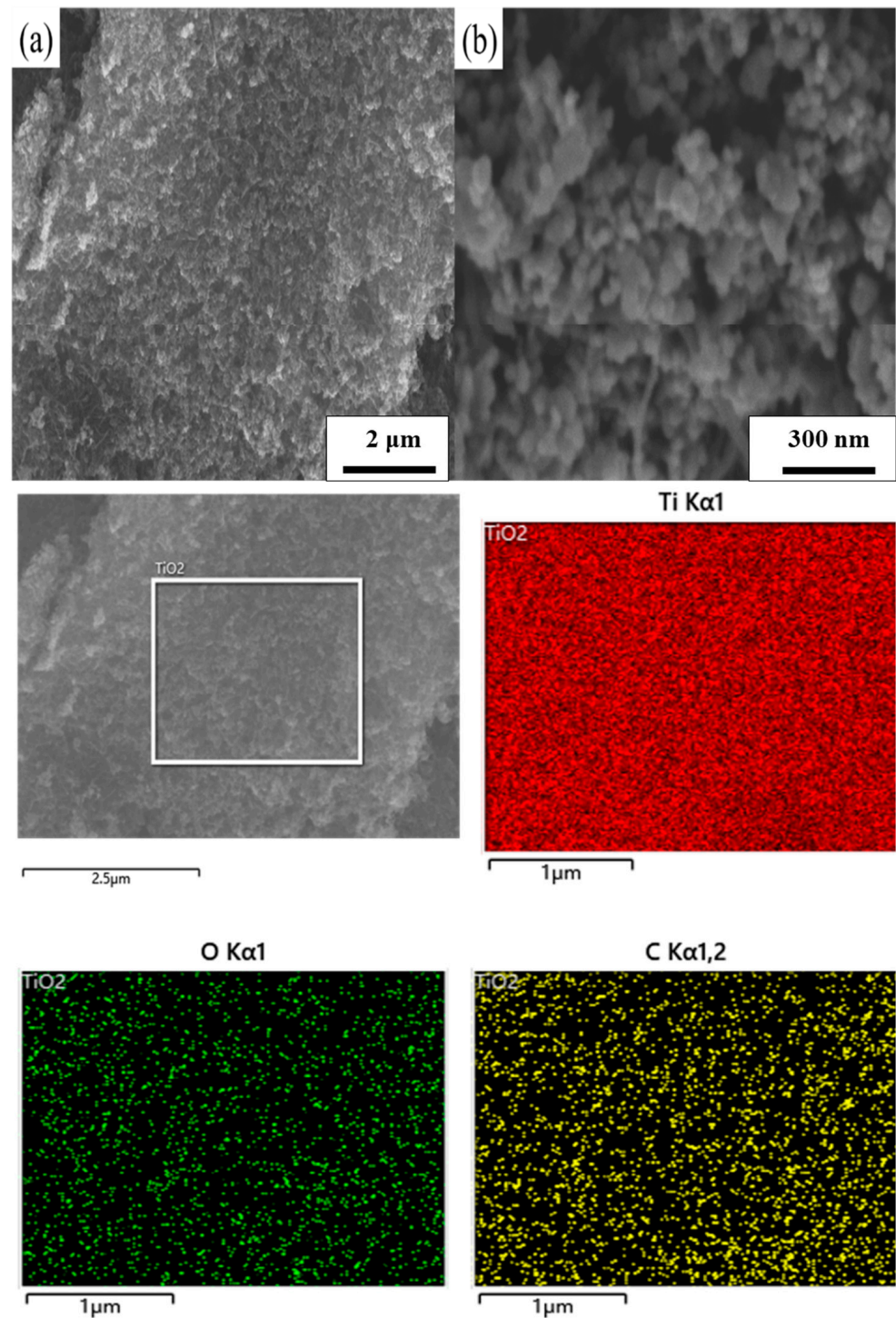


Figure 2. EDS mapping of $\text{TiO}_2/\text{CNT}/\text{CQD}$: (a,b) are SEM images of the $\text{TiO}_2/\text{CNT}/\text{CQD}$ mesoporous composite.

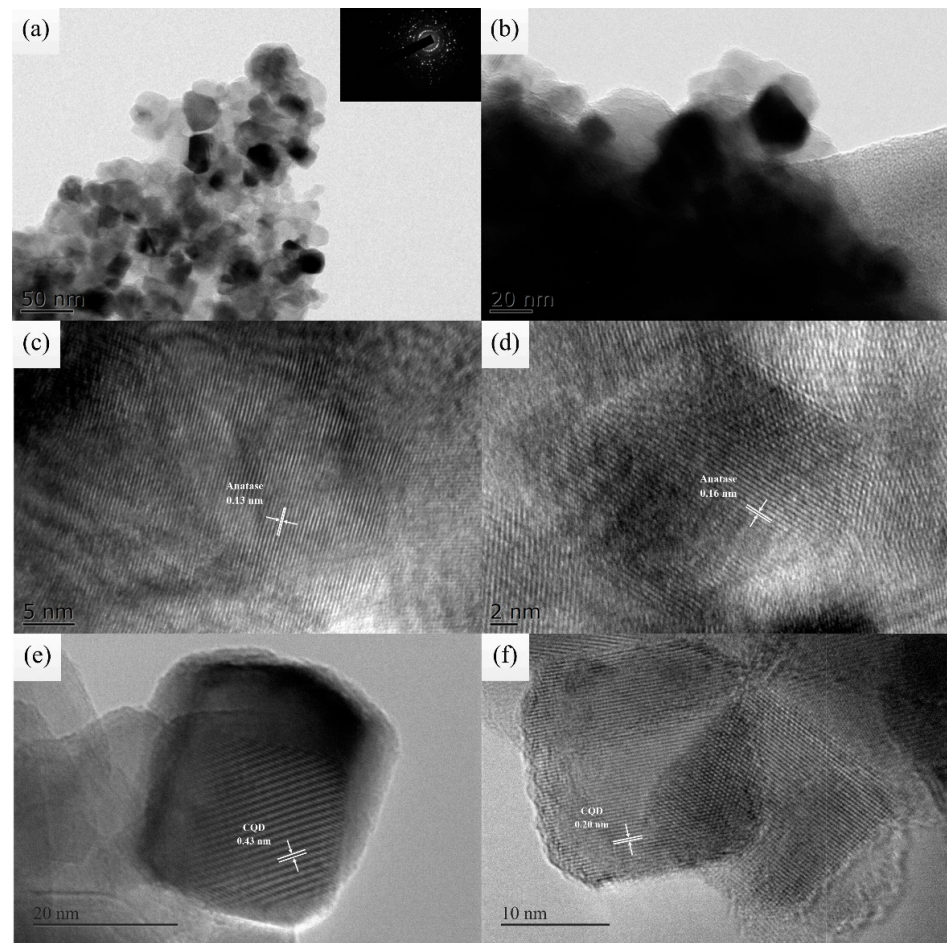


Figure 3. TEM images of the TiO₂/CNT/CQD mesoporous composite: (a,b) are TEM images of the TiO₂/CNT/CQD mesoporous composite, (c,d) are HRTEM images of the anatase phase, (e,f) HRTEM is images of the CQD phase.

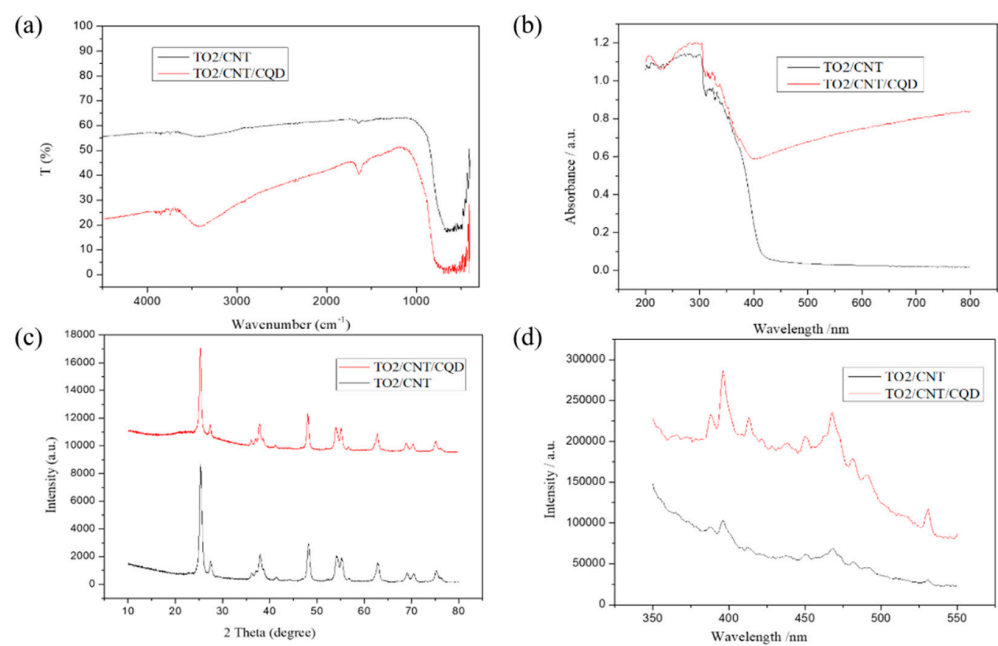


Figure 4. (a) FT-IR spectra, (b) UV-vis, (c) XRD patterns, and (d) photoluminescence spectra of TiO₂/CNT and TiO₂/CNT/CQD mesoporous composites.

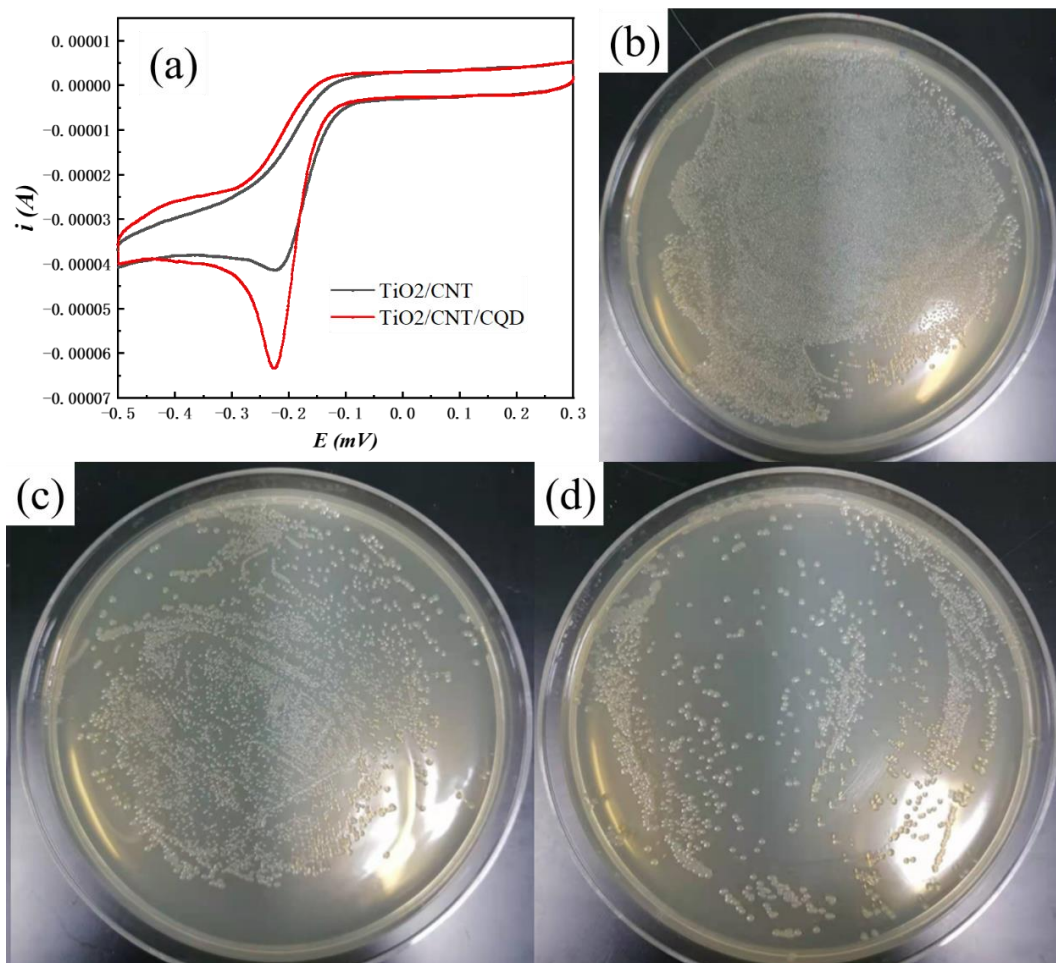


Figure 5. (a) CV curves and anti-bacterial properties of (b) control, (c) TiO₂/CNT, and (d) TiO₂/CNT/CQD using Escherichia coli.

4. Conclusions

The main conclusions were as follows:

- (1) The composites prepared exhibit a large specific surface area of 78.07 m²/g and a pore width of 10–120 nm, indicating that an ultrasonic radiation treatment contributes to forming nanocomposites with a high specific surface area.
- (2) Commercial P25 particles can be prepared into gel films at a low cost by sol-gel ultrasonic radiation.
- (3) TiO₂/CNT/CQD nanocomposites prepared by doping CNT/CQD can significantly improve the visible light absorption efficiency and bactericidal efficiency.

Author Contributions: Conceptualization, H.G., B.D. and Z.Z.; methodology, S.W. and Y.C.; validation, W.K. and L.F.; formal analysis, J.X., L.L. and W.Y.; investigation, J.X. and Z.Z.; writing—original draft preparation, J.X. and H.G.; writing—review and editing, J.X. and Z.Z. All authors have read and agreed to the published version of the manuscript.

Funding: This research received no external funding.

Institutional Review Board Statement: Not applicable.

Informed Consent Statement: Not applicable.

Data Availability Statement: Not applicable.

Conflicts of Interest: The authors declare no conflict of interest.

References

1. Tada, H.; Mitsui, T.; Kiyonaga, T.; Akita, T.; Tanaka, K. All-solid-state Z-scheme in CdS-Au-TiO₂ three-component nanojunction system. *Nat. Mater.* **2006**, *5*, 782–786. [[CrossRef](#)] [[PubMed](#)]
2. Geng, W.; Wang, L.; Yang, X.-Y. Nanocell hybrids for green chemistry. *Trends Biotechnol.* **2022**, *40*, 974–986. [[CrossRef](#)] [[PubMed](#)]
3. Li, H.L.; Luo, S.W.; Zhang, L.Q.; Zhao, Z.L.; Wu, M.; Li, W.H.; Liu, F.Q. Water- and Acid-Sensitive Cu₂O@Cu-MOF Nano Sustained-Release Capsules with Superior Antifouling Behaviors. *ACS Appl. Mater. Interfaces* **2022**, *14*, 1910–1920. [[CrossRef](#)] [[PubMed](#)]
4. Zhao, L.; Guan, B.; Xin, Y.; Huang, X.; Liu, C.; Wu, P.; Liu, Q. A quantitative study on mechanical behavior of Mg alloys with bimodal texture components. *Acta Mater.* **2021**, *214*, 117013. [[CrossRef](#)]
5. Wu, T.W.; Kong, W.H.; Zhang, Y.; Xing, Z.; Zhao, J.X.; Wang, T.; Shi, X.F.; Luo, Y.L.; Sun, X.P. Greatly Enhanced Electrocatalytic N₂ Reduction on TiO₂ via V Doping. *Small Methods* **2019**, *3*, 8. [[CrossRef](#)]
6. Wang, Y.X.; Rao, L.; Wang, P.F.; Shi, Z.Y.; Zhang, L.X. Photocatalytic activity of N-TiO₂/O-doped N vacancy g-C₃N₄ and the intermediates toxicity evaluation under tetracycline hydrochloride and Cr(VI) coexistence environment. *Appl. Catal. B-Environ.* **2020**, *262*, 12. [[CrossRef](#)]
7. Zhao, Z.; Lai, H.S.; Li, H.; Li, L. Preparation and Properties of Graphene Doped TiO₂ Mesoporous Materials for Photocathode Protection. *Int. J. Electrochem. Sci.* **2021**, *16*, 210316. [[CrossRef](#)]
8. Zhao, Z.; Jiang, X.; Li, S.; Li, L.; Feng, Z.; Lai, H. Microstructure Characterization and Battery Performance Comparison of MOF-235 and TiO₂-P25 Materials. *Crystals* **2022**, *12*, 152. [[CrossRef](#)]
9. Feng, Z.Y.; Hurley, B.; Zhu, M.L.; Yang, Z.; Hwang, J.; Buchheit, R. Corrosion Inhibition of AZ31 Mg Alloy by Aqueous Selenite (SeO₃²⁻). *J. Electrochem. Soc.* **2019**, *166*, C520–C529. [[CrossRef](#)]
10. Tripathy, J.; Lee, K.; Schmuki, P. Tuning the Selectivity of Photocatalytic Synthetic Reactions Using Modified TiO₂ Nanotubes. *Angew. Chem.-Int. Ed.* **2014**, *53*, 12605–12608. [[CrossRef](#)]
11. Kong, J.J.; Rui, Z.B.; Ji, H.B. Carbon Nitride Polymer Sensitization and Nitrogen Doping of SrTiO₃/TiO₂ Nanotube Heterostructure toward High Visible Light Photocatalytic Performance. *Ind. Eng. Chem. Res.* **2017**, *56*, 9999–10008. [[CrossRef](#)]
12. Kong, J.J.; Lai, X.D.; Rui, Z.B.; Ji, H.B.; Ji, S.F. Multichannel charge separation promoted ZnO/P25 heterojunctions for the photocatalytic oxidation of toluene. *Chin. J. Catal.* **2016**, *37*, 869–877. [[CrossRef](#)]
13. Xiao, Y.-X.; Ying, J.; Chen, J.-B.; Dong, Y.; Yang, X.; Tian, G.; Wu, J.; Janiak, C.; Ozoemena, K.I.; Yang, X.-Y. Confined Ultrafine Pt in Porous Carbon Fibers and Their N-Enhanced Heavy d-π Effect. *Chem. Mater.* **2022**, *34*, 3705–3714. [[CrossRef](#)]
14. Nie, X.; Wang, J.; Duan, W.; Zhao, Z.; Li, L.; Zhang, Z. One-step preparation of C-doped TiO₂ nanotubes with enhanced photocatalytic activity by a water-assisted method. *Crystengcomm* **2021**, *23*, 3015–3025. [[CrossRef](#)]
15. Feng, Z.; Xu, C.C.; Zhang, D.; Buchheit, R. Corrosion Protective Film Formation on Mg Alloy AZ31 by Exposure to Dilute Selenite Solutions. *Materials* **2021**, *14*, 286. [[CrossRef](#)]
16. Zhao, Z.L.; Li, H.L.; Huang, L.X.; Tan, Y.; Liu, F.Q.; Li, W.H. Preparation of graphene quantum dots-doped TiO₂ nanocomposites via a sol-gel method for photocathodic protection. *Mol. Cryst. Liq. Cryst.* **2021**, *731*, 80–87. [[CrossRef](#)]
17. Asahi, R.; Morikawa, T.; Ohwaki, T.; Aoki, K.; Taga, Y. Visible-light photocatalysis in nitrogen-doped titanium oxides. *Science* **2001**, *293*, 269–271. [[CrossRef](#)]
18. Wang, C.J.; Zhao, Y.L.; Xu, H.; Li, Y.F.; Wei, Y.C.; Liu, J.; Zhao, Z. Efficient Z-scheme photocatalysts of ultrathin g-C₃N₄-wrapped Au/TiO₂-nanocrystals for enhanced visible-light-driven conversion of CO₂ with H₂O. *Appl. Catal. B-Environ.* **2020**, *263*, 13. [[CrossRef](#)]
19. Dong, F.; Guo, S.; Wang, H.; Li, X.; Wu, Z. Enhancement of the Visible Light Photocatalytic Activity of C-Doped TiO₂ Nanomaterials Prepared by a Green Synthetic Approach. *J. Phys. Chem. C* **2011**, *115*, 13285–13292. [[CrossRef](#)]
20. Huang, W.; Wang, X.; Xue, Y.; Yang, Y.; Ao, X. Hybrid nanostructures of mixed-phase TiO₂ for enhanced photoelectrochemical water splitting. *RSC Adv.* **2015**, *5*, 56098–56102. [[CrossRef](#)]
21. Hwang, S.H.; Kim, C.; Jang, J. SnO₂ nanoparticle embedded TiO₂ nanofibers-Highly efficient photocatalyst for the degradation of rhodamine B. *Catal. Commun.* **2011**, *12*, 1037–1041. [[CrossRef](#)]
22. Mei, B.; Pedersen, T.; Malacrida, P.; Bae, D.; Frydendal, R.; Hansen, O.; Vesborg, P.C.K.; Seger, B.; Chorkendorff, I. Crystalline TiO₂: A Generic and Effective Electron-Conducting Protection Layer for Photoanodes and -cathodes. *J. Phys. Chem. C* **2015**, *119*, 15019–15027. [[CrossRef](#)]
23. Tang, C.; Bai, H.; Liu, L.; Zan, X.; Gao, P.; Sun, D.D.; Yan, W. A green approach assembled multifunctional Ag/AgBr/TNF membrane for clean water production & disinfection of bacteria through utilizing visible light. *Appl. Catal. B-Environ.* **2016**, *196*, 57–67. [[CrossRef](#)]
24. Yu, W.; Zheng, B.; Mao, K.; Jiang, J.; Luo, B.; Wu, X.; Tao, T.; Min, X.; Mi, R.; Huang, Z.; et al. Interfacial structure and photocatalytic degradation performance of graphene oxide bridged chitin-modified TiO₂/carbon fiber composites. *J. Clean. Prod.* **2022**, *361*, 132261. [[CrossRef](#)]
25. Wang, J.; Nie, X.; Wang, W.; Zhao, Z.; Li, L.; Zhang, Z. Single-layer graphene-TiO₂ nanotubes array heterojunction as photoanode to enhance the photoelectric of DSSCs. *Optik* **2021**, *242*, 167245. [[CrossRef](#)]
26. Feng, Z.; Li, J.; Ma, J.; Su, Y.; Zheng, X.; Mao, Y.; Zhao, Z. EBSD Characterization of 7075 Aluminum Alloy and Its Corrosion Behaviors in SRB Marine Environment. *J. Mar. Sci. Eng.* **2022**, *10*, 740. [[CrossRef](#)]

27. Ying, J.; Janiak, C.; Xiao, Y.-X.; Wei, H.; Yang, X.-Y.; Su, B.-L. Shape-Controlled Surface-Coating to Pd@Mesoporous Silica Core-Shell Nanocatalysts with High Catalytic Activity and Stability. *Chem. Asian J.* **2018**, *13*, 31–34. [[CrossRef](#)]
28. Shen, L.; Ying, J.; Tian, G.; Jia, M.; Yang, X.-Y. Ultralong PtPd Alloyed Nanowires Anchored on Graphene for Efficient Methanol Oxidation Reaction. *Chem.—Asian J.* **2021**, *16*, 1130–1137. [[CrossRef](#)]
29. Xiao, Y.-X.; Ying, J.; Tian, G.; Tao, Y.; Wei, H.; Fan, S.-Y.; Sun, Z.-H.; Zou, W.-J.; Hu, J.; Chang, G.-G.; et al. Highly dispersed PtPd on graphitic nanofibers and its heavy d- π effect. *Appl. Catal. B Environ.* **2019**, *259*, 118080. [[CrossRef](#)]
30. Xiao, Y.X.; Ying, J.; Tian, G.; Zhang, X.Q.; Janiak, C.; Ozoemena, K.I.; Yang, X.Y. PtPd hollow nanocubes with enhanced alloy effect and active facets for efficient methanol oxidation reaction. *Chem. Commun.* **2021**, *57*, 986–989. [[CrossRef](#)]
31. Li, J.; Li, T.; Zeng, Y.; Chen, C.; Guo, H.; Lei, B.; Zhang, P.; Feng, Z.; Meng, G. A novel sol-gel coating via catechol/lysine polymerization for long-lasting corrosion protection of Mg alloy AZ31. *Colloids Surf. A Physicochem. Eng. Asp.* **2023**, *656*, 130361. [[CrossRef](#)]
32. Zheng, H.Y.; Guo, Y.C.; Shen, F.M. Production of titanium powder by metallothermic reduction of TiO₂ in cold pressed pellets. *J. Cent. South Univ.* **2021**, *28*, 48–57. [[CrossRef](#)]
33. Xue, S.G.; Tang, L.; Tang, T.; Zhang, F.; Lyu, H.G.; Liu, H.Y.; Jiang, J.; Huang, Y.H. Identifying the active sites in C-N codoped TiO₂ electrode for electrocatalytic water oxidation to produce H₂O₂. *J. Cent. South Univ.* **2022**, *29*, 3016–3029. [[CrossRef](#)]
34. Fan, B.Y.; Liu, H.B.; Wang, Z.H.; Zhao, Y.W.; Yang, S.; Lyu, S.Y.; Xing, A.; Zhang, J.; Li, H.; Liu, X.Y. Ferroelectric polarization-enhanced photocatalytic performance of heterostructured BaTiO₃@TiO₂ via interface engineering. *J. Cent. South Univ.* **2021**, *28*, 3778–3789. [[CrossRef](#)]
35. Nong, S.; Dong, W.; Yin, J.; Dong, B.; Lu, Y.; Yuan, X.; Wang, X.; Bu, K.; Chen, M.; Jiang, S.; et al. Well-Dispersed Ruthenium in Mesoporous Crystal TiO₂ as an Advanced Electrocatalyst for Hydrogen Evolution Reaction. *J. Am. Chem. Soc.* **2018**, *140*, 5719–5727. [[CrossRef](#)]
36. Xiao, Y.X.; Ying, J.; Tian, G.; Yang, X.; Zhang, Y.X.; Chen, J.B.; Wang, Y.; Symes, M.D.; Ozoemena, K.I.; Wu, J.; et al. Hierarchically Fractal PtPdCu Sponges and their Directed Mass- and Electron-Transfer Effects. *Nano Lett.* **2021**, *21*, 7870–7878. [[CrossRef](#)]
37. Shen, L.; Ying, J.; Ozoemena, K.I.; Janiak, C.; Yang, X.-Y. Confinement Effects in Individual Carbon Encapsulated Nonprecious Metal-Based Electrocatalysts. *Adv. Funct. Mater.* **2022**, *32*, 2110851. [[CrossRef](#)]
38. Zhao, Z.; Liu, X.; Li, S.; Mao, Y.; Feng, Z.; Ke, W.; Liu, F. Study on Strengthening and Toughening of Mechanical Properties of Mg-Li Alloy by Adding Non-Rare-Earth Elements Al and Si. *JOM* **2022**, *74*, 2554–2565. [[CrossRef](#)]
39. Bai, C.; Xiang, J.; Zhao, Z.; Luo, S.; Li, L. Improvement of hydrogen production performance by in situ doping of carbon nanotubes into TiO₂ materials. *J. Nanopart. Res.* **2022**, *24*, 61. [[CrossRef](#)]
40. Yang, F.; Wen, L.Y.; Peng, Q.; Zhao, Y.; Xu, J.; Hu, M.L.; Zhang, S.F.; Yang, Z.Q. Prediction of structural and electronic properties of Cl-2 adsorbed on TiO₂(100) surface with C or CO in fluidized chlorination process: A first-principles study. *J. Cent. South Univ.* **2021**, *28*, 29–38. [[CrossRef](#)]
41. Nie, X.J.; Yin, S.Q.; Duan, W.C.; Zhao, Z.L.; Li, L.; Zhang, Z.Q. Recent Progress in Anodic Oxidation of TiO₂ Nanotubes and Enhanced Photocatalytic Performance: A Short Review. *Nano* **2021**, *16*, 2130002. [[CrossRef](#)]
42. Zhang, R.; Wu, H.; Lin, D.D.; Pan, W. Preparation of Necklace-Structured TiO₂/SnO₂ Hybrid Nanofibers and Their Photocatalytic Activity. *J. Am. Ceram. Soc.* **2009**, *92*, 2463–2466. [[CrossRef](#)]
43. Zhao, J.; Zhang, J.L.; Wang, L.; Lyu, S.S.; Ye, W.L.; Xu, B.B.; Qiu, H.; Chen, L.X.; Gu, J.W. Fabrication and investigation on ternary heterogeneous MWCNT@TiO₂-C fillers and their silicone rubber wave-absorbing composites. *Compos. Pt. A-Appl. Sci. Manuf.* **2020**, *129*, 8. [[CrossRef](#)]
44. Hu, G.; Xiao, Y.; Ying, J. Nano-SiO₂ and Silane Coupling Agent Co-Decorated Graphene Oxides with Enhanced Anti-Corrosion Performance of Epoxy Composite Coatings. *Int. J. Mol. Sci.* **2021**, *22*, 11087. [[CrossRef](#)]
45. Zheng, J.Y.; Lyu, Y.H.; Wang, R.L.; Xie, C.; Zhou, H.J.; Jiang, S.P.; Wang, S.Y. Crystalline TiO₂ protective layer with graded oxygen defects for efficient and stable silicon-based photocathode. *Nat. Commun.* **2018**, *9*, 3572. [[CrossRef](#)]
46. Zeng, L.; Cui, H.; Peng, H.; Sun, X.; Liu, Y.; Huang, J.; Lin, X.; Guo, H.; Li, W.-H. Oleophobic interaction mediated slippery organogels with ameliorated mechanical performance and satisfactory fouling-resistance. *J. Mater. Sci. Technol.* **2022**, *121*, 227–235. [[CrossRef](#)]
47. Liu, Y.; Cui, H.; Wang, X.; Ouyang, G.; Guo, H. Hydrogels with Reversible Heat-Trained Toughness for Convenient Manufacture. *Adv. Mater. Technol.* **2022**, *110*, 2201346. [[CrossRef](#)]
48. Zeng, L.; Lin, X.; Li, P.; Liu, F.-Q.; Guo, H.; Li, W.-H. Recent advances of organogels: From fabrications and functions to applications. *Prog. Org. Coat.* **2021**, *159*, 106417. [[CrossRef](#)]
49. Zhou, W.; Sun, F.; Pan, K.; Tian, G.; Jiang, B.; Ren, Z.; Tian, C.; Fu, H. Well-Ordered Large-Pore Mesoporous Anatase TiO₂ with Remarkably High Thermal Stability and Improved Crystallinity: Preparation, Characterization, and Photocatalytic Performance. *Adv. Funct. Mater.* **2011**, *21*, 1922–1930. [[CrossRef](#)]

Disclaimer/Publisher’s Note: The statements, opinions and data contained in all publications are solely those of the individual author(s) and contributor(s) and not of MDPI and/or the editor(s). MDPI and/or the editor(s) disclaim responsibility for any injury to people or property resulting from any ideas, methods, instructions or products referred to in the content.